

# Novel Ruthenium(II) N-Heterocyclic Carbene Complexes as Catalyst Precursors for the Ring-Opening Metathesis Polymerization (ROMP) of Enantiomerically Pure Monomers: X-ray Structures, Reactivity, and Quantum Chemical Considerations

Michael R. Buchmeiser,<sup>\*[a,b]</sup> Dongren Wang,<sup>[a]</sup> Yan Zhang,<sup>[a]</sup> Sergej Naumov,<sup>[a]</sup> and Klaus Wurst<sup>[c]</sup>

**Keywords:** Carbene ligands / Ruthenium / ROMP / Quantum chemistry

Four chiral, enantiomerically pure monomers, *exo,exo*-*N,N*-(norborn-5-ene-2,3-dicarbimido)-*L*-valine ethyl ester (*exo*-**1**), *endo,endo*-*N,N*-(norborn-5-ene-2,3-dicarbimido)-*L*-valine ethyl ester (*endo*-**1**), *exo,exo*-*N,N*-(norborn-5-ene-2,3-dicarbimido)-*L*-valine-*tert*-butylamide (*exo*-**2**), and *endo,endo*-*N,N*-(norborn-5-ene-2,3-dicarbimido)-*L*-valine-*tert*-butylamide (*endo*-**2**), were subjected to ring-opening metathesis polymerization (ROMP) with Ru(CF<sub>3</sub>CO<sub>2</sub>)<sub>2</sub>(IMesH<sub>2</sub>)(*p*-cymene) (**3**), Ru(CF<sub>3</sub>CO<sub>2</sub>)<sub>2</sub>(IMes)(*p*-cymene) (**4**), RuCl<sub>2</sub>(IMes)(*p*-cymene) (**5**), Ru(PCy<sub>3</sub>)(CF<sub>3</sub>CO<sub>2</sub>)<sub>2</sub>(*p*-cymene) (**6**), Ru(CF<sub>3</sub>CO<sub>2</sub>)<sub>2</sub>(*p*-cymene)-CF<sub>3</sub>COOAgPCy<sub>3</sub> (**6a**), Ru(CF<sub>3</sub>CO<sub>2</sub>)<sub>2</sub>(PPh<sub>3</sub>)(*p*-cymene) (**7**), Ru(CF<sub>3</sub>CO<sub>2</sub>)<sub>2</sub>(IMes)(PhNC)<sub>3</sub> (**8**), and Ru(CF<sub>3</sub>CO<sub>2</sub>)<sub>2</sub>(IMesH<sub>2</sub>)(PhNC)<sub>3</sub> (**9**) (IMes = 1,3-dimesitylimidazol-2-ylidene, IMesH<sub>2</sub> = 1,4-dimesityl-4,5-dihydroimidazol-2-ylidene, PCy<sub>3</sub> = tricyclohexylphosphane). X-ray struc-

tures of precatalysts **3** and **6–9** are presented. Compounds **3** and **4** displayed significant ROMP activity, allowing for the controlled, yet nonliving synthesis of the corresponding polymers with polydispersity indices (PDIs) in the range of 1.17–2.14. In all cases the *exo* isomers of compounds **1** and **2** were polymerized by preference. While poly(*endo*-**1**) was formed in an all-*trans* form, poly(*exo*-**1**) and poly(*exo*-**2**) were produced in their *cis/trans* forms with a *cis* content of around 40%. Calculations carried out at the B3LYP/LACVP\* level suggest two possible mechanisms for the increased reactivity of the 2,3-R<sub>2</sub>-*exo,exo* isomers of norborn-5-ene-2,3-dicarbimido derivatives resulting in the formation of the ROMP-active Ru<sup>IV</sup> alkylidene.

(© Wiley-VCH Verlag GmbH & Co. KGaA, 69451 Weinheim, Germany, 2007)

## Introduction

The first reports on the activity of ruthenium(II) complexes in ring-opening metathesis polymerization (ROMP) were published some 15 years ago<sup>[1]</sup> and may certainly be regarded as the basis for the development of well-defined ruthenium(IV)-alkylidene complexes.<sup>[1,2]</sup> In 1997, Hafner et al. reported on the photo- and thermal activation of Ru<sup>II</sup> and Os<sup>II</sup> arene complexes of the general formula MCl<sub>2</sub>(PR<sub>3</sub>)(*p*-cymene) (M = Ru, Os) in the polymerization of norborn-2-ene.<sup>[3]</sup> Thermal initiation of the ROMP of norborn-2-ene was also observed by Lindner et al. for Ru-

(arene)H[P–O] complexes.<sup>[4]</sup> Noels et al. showed that complexes of the general formula RuCl<sub>2</sub>(PCy<sub>3</sub>)(arene) can be activated by treatment with diazo compounds to form ROMP-active Grubbs-type catalysts.<sup>[5]</sup> RuCl<sub>2</sub>(IMes)(*p*-cymene) (**5**) (IMes = 1,3-dimesitylimidazol-2-ylidene) was first reported by Nolan et al., who showed that this complex was capable of performing ring-closing metathesis (RCM) reactions.<sup>[6]</sup> Later, Dixneuf et al. reported on the *in situ* formation of **5** and RuCl<sub>2</sub>(IMesH<sub>2</sub>)(*p*-cymene) (IMesH<sub>2</sub> = 1,4-dimesityl-4,5-dihydroimidazol-2-ylidene) and their use in RCM, enyne metathesis reactions,<sup>[7–10]</sup> and later in ROMP.<sup>[11]</sup> Noels et al. suggested the use of **5**, RuCl<sub>2</sub>(IMesH<sub>2</sub>)(*p*-cymene), and derivatives thereof as photoinitiators that can be activated by visible light.<sup>[12,13]</sup> However, in view of their inherent activity even *in the absence of light*,<sup>[14]</sup> they appear less suitable for these applications. As a matter of fact, calculations at the B3LYP/LACVP\* level indicate a dissociation energy  $E_{\text{diss}}$  of only 8.7 kcal/mol for the dissociation of the *p*-cymene ligand in RuCl<sub>2</sub>(IMesH<sub>2</sub>)(*p*-cymene).

In an ongoing project we are interested in the synthesis of novel latent metathesis catalysts<sup>[15,16]</sup> that may be converted into the active species in the presence of a monomer either thermally or by the action of (UV) light.<sup>[14]</sup> Key properties of such compounds are high thermal stability of

[a] Leibniz-Institut für Oberflächenmodifizierung e.V. (IOM), Permoserstr. 15, 04318 Leipzig, Germany  
Fax: +49-341-235-2584  
E-mail: michael.buchmeiser@iom-leipzig.de  
dongren.wang@iom-leipzig.de  
chem\_yzhang@yahoo.com  
sergej.naumov@iom-leipzig.de

[b] Institut für Technische Chemie, Universität Leipzig, Linnéstr. 3, 04103 Leipzig, Germany

[c] Institut für Allgemeine, Anorganische und Theoretische Chemie, Leopold-Franzens-Universität Innsbruck, Innrain 52 a, 6020 Innsbruck, Austria  
E-mail: klaus.wurst@uibk.ac.at

Supporting information for this article is available on the WWW under <http://www.eurjic.org> or from the author.

the precatalyst at least up to 45 °C and prolonged storability of ready-to-use monomer–precatalyst mixtures up to this temperature. Vice versa, either by the action of UV light or by thermal treatment, the precatalyst should, together with the monomer, form the active species to initiate ROMP. Despite selected reports on such systems,<sup>[3,17–20]</sup> these suffer from drawbacks such as thermal or visible light activation and significant metathesis activity *at room temperature and below*. In view of the pronounced changes in reactivity observed for bis(trifluoroacetate)-derived Grubbs and Grubbs–Hoveyda systems,<sup>[21–27]</sup> we were interested to what extent the replacement of the chlorine groups by trifluoroacetate groups would have influence on the ROMP activity of the resulting precatalysts. Instead of using norborn-2-ene, which is polymerized to some extent by virtually any metathesis catalyst, we focused on more complex molecules. On the basis of previous reports on the superiority of *exo* isomers in ROMP,<sup>[11]</sup> we prepared enantiomerically pure *exo* and *endo* isomers of two monomers, *exo,exo-N,N*-(norborn-5-ene-2,3-dicarbimido)-L-valine ethyl ester (*exo-1*), *endo,endo-N,N*-(norborn-5-ene-2,3-dicarbimido)-L-valine ethyl ester (*endo-1*), *exo,exo-N,N*-(norborn-5-ene-2,3-dicarbimido)-L-valine-*tert*-butylamide (*exo-2*), *endo,endo-N,N*-(norborn-5-ene-2,3-dicarbimido)-L-valine-*tert*-butylamide (*endo-2*) and investigated their polymerization using Ru(CF<sub>3</sub>CO<sub>2</sub>)<sub>2</sub>(IMesH<sub>2</sub>)(*p*-cymene) (**3**), Ru(CF<sub>3</sub>CO<sub>2</sub>)<sub>2</sub>(IMes)(*p*-cymene) (**4**), RuCl<sub>2</sub>(IMes)(*p*-cymene) (**5**), Ru(PCy<sub>3</sub>)(CF<sub>3</sub>CO<sub>2</sub>)<sub>2</sub>(*p*-cymene) (**6**), Ru(CF<sub>3</sub>CO<sub>2</sub>)<sub>2</sub>(*p*-cymene)·CF<sub>3</sub>COOAgPCy<sub>3</sub> (**6a**), Ru(CF<sub>3</sub>CO<sub>2</sub>)<sub>2</sub>(PPh<sub>3</sub>)(*p*-cymene) (**7**), Ru(CF<sub>3</sub>CO<sub>2</sub>)<sub>2</sub>(IMes)(PhNC)<sub>3</sub> (**8**), and Ru(CF<sub>3</sub>CO<sub>2</sub>)<sub>2</sub>(IMesH<sub>2</sub>)(PhNC)<sub>3</sub> (**9**) (IMes = 1,3-dimesitylimidazol-2-ylidene, IMesH<sub>2</sub> = 1,3-dimesityl-4,5-dihydroimidazol-2-ylidene, PCy<sub>3</sub> = tricyclohexylphosphane). In addition, the structure of the final polymers was investigated. Finally, we performed theoretical calculations at the B3LYP/LACVP\*

level and propose a model that explains the superior reactivity of *exo* isomers compared to their *endo* analogues in ROMP.

## Results and Discussion

### Synthesis of Monomers and Catalyst Precursors

The synthesis of the *endo* monomers *endo-1* and *endo-2*,<sup>[28]</sup> the CF<sub>3</sub>COO-derived precatalysts **3**, **4**, **8**, and **9**,<sup>[14]</sup> as well as of precatalyst **5**,<sup>[6]</sup> is described elsewhere. Monomer *exo-1* was prepared by esterification of *exo,exo*-(norborn-5-ene-2,3-dicarbimido)-L-valine with ethanol. Monomer *exo-2* was synthesized by reaction of L-valine-*exo,exo-N,N*-(norborn-5-ene-5,6-dicarbimide) with dicyclohexyldicarbodiimide (DCC) followed by the reaction of *tert*-butylamine. All structures are shown in Figure 1. In addition to the data already reported, the X-ray structures of compounds **3**, **6a**, **7**, **8**, and **9** are presented here. Thus, compound **3** crystallizes in the triclinic space group *P* $\bar{1}$  with  $a = 11.3770(4)$  Å,  $b = 12.1632(5)$  Å,  $c = 14.5978(6)$  Å,  $\alpha = 104.636(2)^\circ$ ,  $\beta = 96.217(2)^\circ$ ,  $\gamma = 113.276(2)^\circ$ ,  $Z = 2$ . The distance Ru(1)–C(11) is 2.109(2) Å; the complex exists in a distorted octahedral form (Figure 2).

Precatalyst **6** was prepared from [RuCl<sub>2</sub>(*p*-cymene)]<sub>2</sub> by reaction with 2 equiv. of PCy<sub>3</sub> followed by reaction with 2 equiv. of CF<sub>3</sub>COOAg. The compound crystallizes as the CF<sub>3</sub>COOAg·PCy<sub>3</sub> adduct **6a** in the triclinic space group *P* $\bar{1}$  with  $a = 10.2007(4)$  Å,  $b = 13.8886(4)$  Å,  $c = 14.9130(6)$  Å,  $\alpha = 107.497(2)^\circ$ ,  $\beta = 94.569(2)^\circ$ ,  $\gamma = 95.552(2)^\circ$ ,  $Z = 2$ . The complex again exists with a distorted octahedral coordination for the Ru and a distorted tetrahedral coordination for the Ag center (Figure 3).

In a similar manner, precatalyst **7** was prepared from [RuCl<sub>2</sub>(*p*-cymene)]<sub>2</sub> by reaction with 2 equiv. of PPh<sub>3</sub> fol-

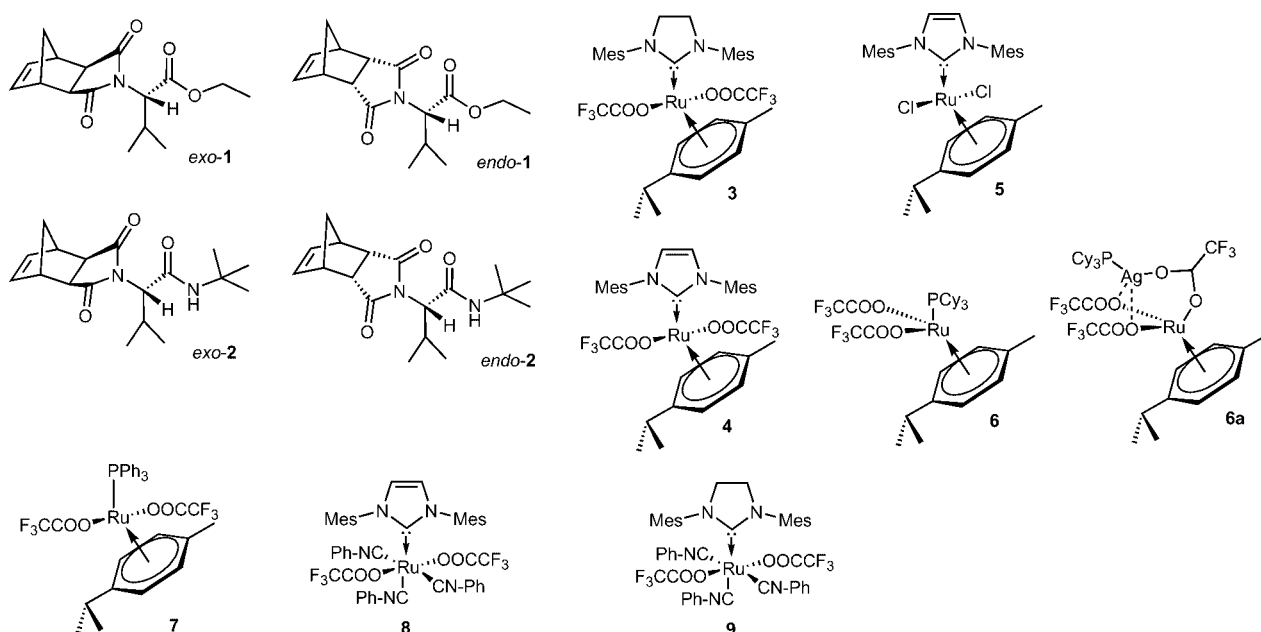


Figure 1. Monomers *exo-1*, *endo-1*, *exo-2*, *endo-2*, and precatalysts **3–10** used.

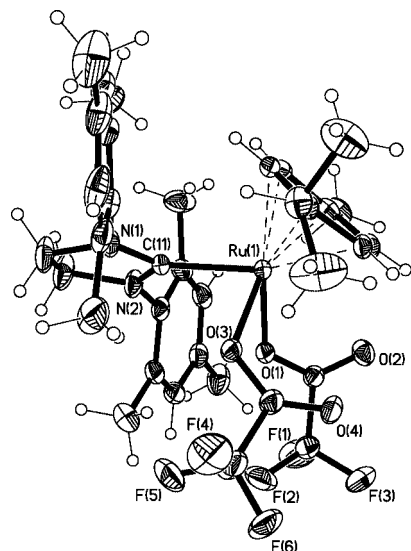


Figure 2. X-ray structure of **3**. Selected bond lengths [Å] and angles [°]: Ru(1)–C(11) 2.109(2), Ru(1)–O(1) 2.113(2), Ru(1)–O(3) 2.113(2), Ru(1)–C(5) 2.174(3), Ru(1)–C(6) 2.175(3), Ru(1)–C(4) 2.208(3), Ru(1)–C(1) 2.216(3), Ru(1)–C(2) 2.262(3), Ru(1)–C(3) 2.266(2); C(11)–Ru(1)–O(1) 87.37(9), C(11)–Ru(1)–O(3) 82.52(9), O(1)–Ru(1)–O(3) 76.20(8).

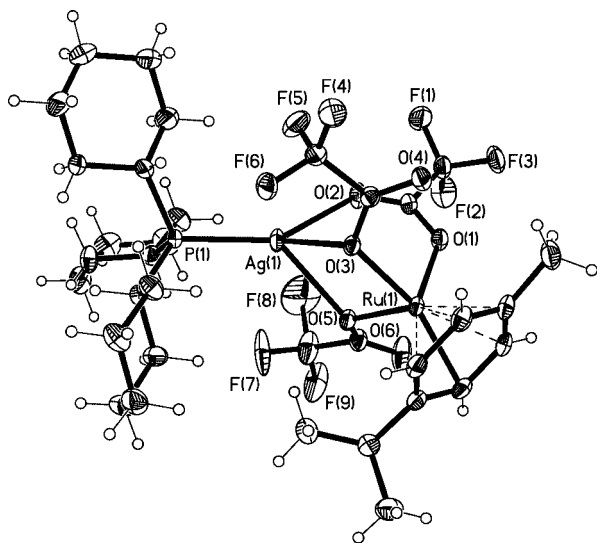


Figure 3. X-ray structure of **6a**. Selected bond lengths [Å] and angles [°]: Ru(1)–O(1) 2.1082(18), Ru(1)–O(3) 2.121(2), Ru(1)–O(5) 2.131(2), Ru(1)–C(3) 2.155(3), Ru(1)–C(2) 2.156(3), Ru(1)–C(5) 2.166(2), Ru(1)–C(1) 2.168(3), Ru(1)–C(6) 2.169(2), Ru(1)–C(4) 2.185(2), Ag(1)–O(2) 2.348(2), Ag(1)–P(1) 2.362(1), Ag(1)–O(3) 2.478(2), Ag(1)–O(5) 2.507(2); O(1)–Ru(1)–O(3) 86.44(7), O(1)–Ru(1)–O(5) 84.57(7), O(3)–Ru(1)–O(5) 80.29(6), O(2)–Ag(1)–P(1) 143.72(5), O(2)–Ag(1)–O(3) 74.93(6), P(1)–Ag(1)–O(3) 132.63(4), O(2)–Ag(1)–O(5) 75.94(6), P(1)–Ag(1)–O(5) 132.12(4), O(3)–Ag(1)–O(5) 66.70(5).

lowed by reaction with 2 equiv. of  $\text{CF}_3\text{COOAg}$ . Compound **7** crystallized in the monoclinic space group  $C2/c$  with  $a = 27.0985(3)$  Å,  $b = 14.4321(4)$  Å,  $c = 20.3053(5)$  Å,  $\alpha = \gamma = 90^\circ$ ,  $\beta = 109.654(2)^\circ$ ,  $Z = 8$  (Figure 4).

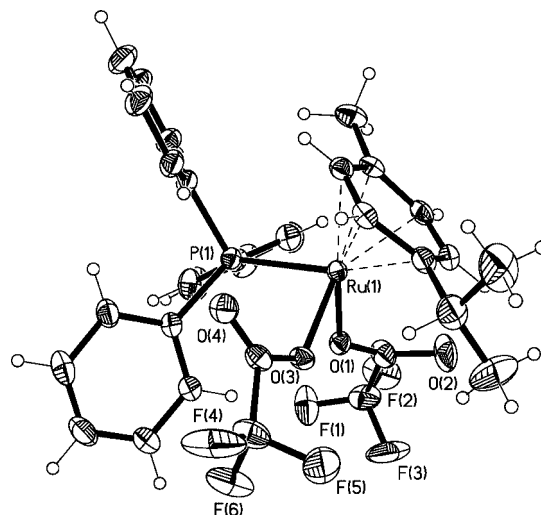


Figure 4. X-ray structure of **7**. Selected bond lengths [Å] and angles [°]: Ru(1)–O(3) 2.093(2), Ru(1)–O(1) 2.107(2), Ru(1)–C(6) 2.169(2), Ru(1)–C(5) 2.179(2), Ru(1)–C(3) 2.189(2), Ru(1)–C(2) 2.230(3), Ru(1)–C(4) 2.240(2), Ru(1)–C(1) 2.265(3), Ru(1)–P(1) 2.3654(7); O(3)–Ru(1)–O(1) 78.89(7), O(3)–Ru(1)–P(1) 89.59(5), O(1)–Ru(1)–P(1) 79.71(5).

Again, the complex exists with a distorted octahedral coordination of the Ru core. Compound **8** was prepared by reaction of **4** with excess phenylisocyanide.<sup>[14]</sup> It crystallizes in the orthorhombic space group  $P2_12_12_1$  with  $a = 10.8932(2)$  Å,  $b = 16.4398(4)$  Å,  $c = 26.9136(7)$  Å,  $\alpha = \beta = \gamma = 90^\circ$ ,  $Z = 4$  (Figure 5). The Ru center again shows a slightly distorted octahedral coordination sphere with all angles close to 90 and 180°, respectively. One of the three phenylisocyanide ligands is arranged in a position *trans* to

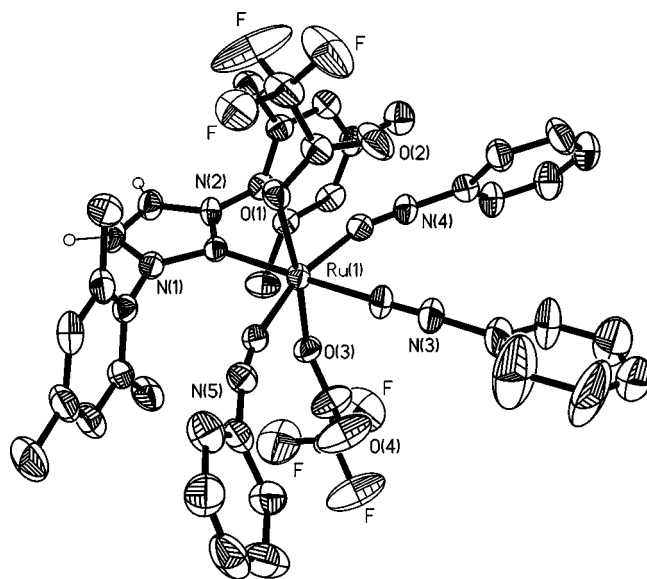


Figure 5. X-ray structure of **8**. Selected bond lengths [Å] and angles [°]: Ru(1)–C(27) 1.968(6), Ru(1)–C(20) 1.980(7), Ru(1)–C(34) 1.986(7), Ru(1)–O(3) 2.091(4), Ru(1)–O(1) 2.096(4), Ru(1)–C(1) 2.112(5); C(20)–Ru(1)–C(34) 164.9(2), O(3)–Ru(1)–O(1) 172.1(2), C(27)–Ru(1)–C(1) 178.5(2), Ru(1)–C(20)–N(3) 166.1(5), Ru(1)–C(27)–N(4) 177.2(6), Ru(1)–C(34)–N(5) 162.3(5).

the N-heterocyclic carbene ligand. The two trifluoroacetate ligands are *trans* to each other.

Because of its structural similarity to **8**, compound **9** again crystallizes in the orthorhombic space group  $P2_12_12_1$  with  $a = 10.8403(2)$  Å,  $b = 16.5038(3)$  Å,  $c = 27.1075(4)$  Å,  $\alpha = \beta = \gamma = 90^\circ$ ,  $Z = 4$  (Figure 6). The arrangement of the two phenylisocyanide and trifluoroacetate ligands is identical to that in **8**.

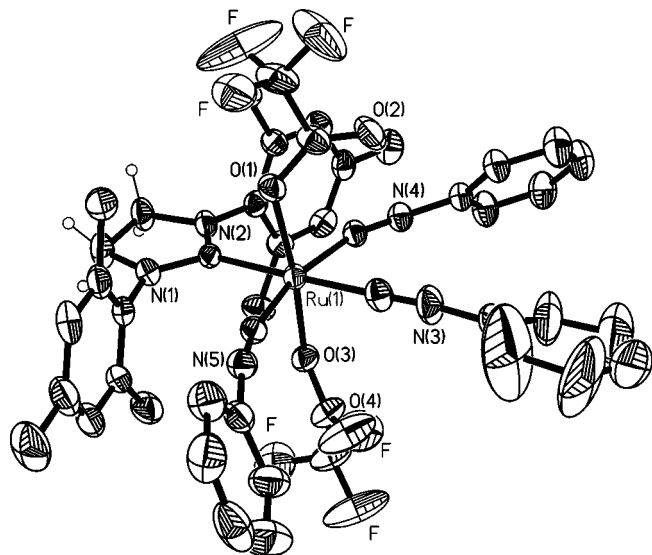


Figure 6. X-ray structure of **9**. Selected bond lengths [Å] and angles [°]: Ru(1)–C(27) 1.967(5), Ru(1)–C(20) 1.986(5), Ru(1)–C(34) 1.986(5), Ru(1)–O(3) 2.096(3), Ru(1)–O(1) 2.102(3), Ru(1)–C(1) 2.123(4), C(20)–Ru(1)–C(34) 164.4(2); O(3)–Ru(1)–O(1) 172.6(1), C(27)–Ru(1)–C(1) 178.5(2), Ru(1)–C(20)–N(3) 166.1(4), Ru(1)–C(27)–N(4) 178.4(5), Ru(1)–C(34)–N(5) 161.8(4).

### Reactivity in ROMP

All precatalysts, **3–9**, were investigated for their activity in ROMP using the monomers *exo-1*, *endo-1*, *exo-2*, and

*endo-2*. In all cases, only precatalysts **3** and **4** were found to possess significant polymerization activity. Poly(*endo-1*) was prepared by the action of both precatalysts **3** and **4** (Table 1, entries 1–13) in the molecular weight range of 25000–160000 g/mol and polydispersity indices (PDIs) in the range of 1.17–1.54. A graph of the number of equivalents of the monomer with respect to the precatalyst ( $N$ ) versus  $M_n$  illustrates these results (Figure 7).

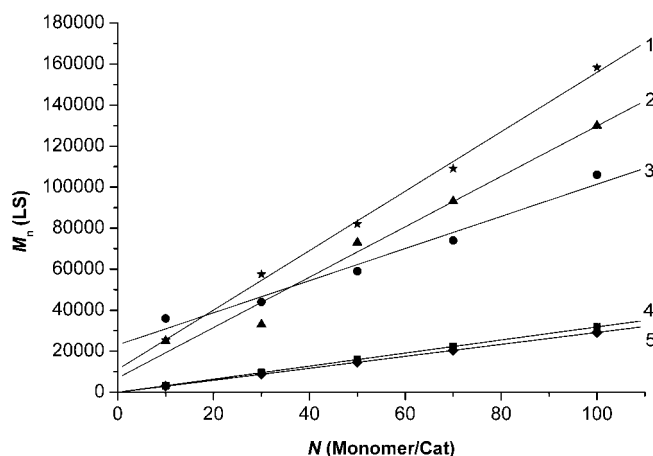


Figure 7. Plot of  $M_n$  vs. number of monomer equivalents ( $N$ ): 1: precatalyst **3** with *endo-1*; 2: precatalyst **4** with *exo-2*; 3: precatalyst **3** with *exo-2*; 4: calculated values for monomer **2**; 5: calculated values for monomer **1**.

As can be deduced therefrom, polymerization proceeds in a *controlled* manner, that is, the values of  $M_n$  increase linearly with increasing  $N$ . The stepwise synthesis of poly(*endo-1*)<sub>100</sub> (Table 1, entry 13) yields a polymer similar to the one prepared in a one-step procedure (Table 1, entry 9), however with higher PDI. This suggests that the polymerization does not proceed in a truly living<sup>[29]</sup> manner. The fact that the values for  $M_n$  as determined by light scattering

Table 1. Polymerization results for *endo-1* and *exo-1* catalyzed by the action of precatalysts **3** and **4**. Solvent:  $\text{ClCH}_2\text{CH}_2\text{Cl}$ , 70 °C, 8 h.

Entry	Monomer	Catalyst	$N$	$M_n$ (theor.) <sup>[a]</sup>	$M_n$ (LS)	PDI	Yield [%]
1	<i>endo-1</i>	<b>4</b>	10	2913	–	–	oligomer
2	<i>endo-1</i>	<b>4</b>	30	8740	–	–	oligomer
3	<i>endo-1</i>	<b>4</b>	50	14567	40000	1.37	10
4	<i>endo-1</i>	<b>4</b>	70	20393	85000	1.25	23
5	<i>endo-1</i>	<b>4</b>	100	29134	91000	1.38	43
6	<i>endo-1</i>	<b>3</b>	10	2913	25300	1.17	52
7	<i>endo-1</i>	<b>3</b>	30	8740	57500	1.24	72
8	<i>endo-1</i>	<b>3</b>	50	14567	82000	1.34	80
9	<i>endo-1</i>	<b>3</b>	70	20393	109000	1.35	80
10	<i>endo-1</i>	<b>3</b>	100	29134	158300	1.38	85
11	<i>endo-1</i>	<b>3</b>	50 <sup>[b]</sup>	14567	50800	1.40	48
12	<i>endo-1</i>	<b>3</b>	50	14567	88000	1.39	<sup>[c]</sup>
13	<i>endo-1</i>	<b>3</b>	50–100	29134	166000	1.54	80
14	<i>exo-1</i>	<b>4</b>	10	2913	–	–	oligomer
15	<i>exo-1</i>	<b>4</b>	30	8740	–	–	oligomer
16	<i>exo-1</i>	<b>4</b>	50	14567	64500	2.00	42
17	<i>exo-1</i>	<b>4</b>	70	20393	55700	1.94	60
18	<i>exo-1</i>	<b>4</b>	100	29134	152000	1.71	78
19	<i>exo-1</i>	<b>3</b>	50	14567	58600	2.09	100
20	<i>exo-1</i>	<b>3</b>	100	29134	116000	2.14	100

[a] Without end groups. [b] 1 equiv. of pyridine. [c] Taken from experiment entry 13 prior to addition of second 50 equiv. of monomer.

are much higher than the calculated ones also suggests a nonquantitative initiation of the precatalysts. Not unexpectedly, addition of pyridine (Table 1, entry 11) reduces the molecular weight of the polymer.

It is worth noting that **3** is far more reactive than **4**, as illustrated by the comparably low yields ( $\leq 43\%$ ) obtained with the latter. The lower activity of **4** in comparison to **3** may be rationalized by the fact that precatalyst **3** is believed

Table 2. Polymerization results for *endo-2* and *exo-2* catalyzed by the action of precatalysts **3** and **4**. Solvent:  $\text{ClCH}_2\text{CH}_2\text{Cl}$ , 70 °C, 8 h.

Entry	Monomer	Catalyst	<i>N</i>	$M_n$ (theor.) <sup>[a]</sup>	$M_n$ (LS)	PDI	Yield [%]
1	<i>endo-2</i>	<b>4</b>	10	3182	insoluble	–	8
2	<i>endo-2</i>	<b>4</b>	30	9546	insoluble	–	10
3	<i>endo-2</i>	<b>4</b>	50	15910	insoluble	–	10
4	<i>endo-2</i>	<b>4</b>	70	22274	insoluble	–	15
5	<i>endo-2</i>	<b>4</b>	100	31820	insoluble	–	18
6	<i>endo-2</i>	<b>3</b>	50	15910	–	–	oligomer
7	<i>endo-2</i>	<b>3</b>	100	31820	–	–	oligomer
8	<i>exo-2</i>	<b>4</b>	10	3182	25000	1.83	52
9	<i>exo-2</i>	<b>4</b>	30	9546	33000	2.05	53
10	<i>exo-2</i>	<b>4</b>	50	15910	73000	1.91	61
11	<i>exo-2</i>	<b>4</b>	70	22274	93200	1.88	75
12	<i>exo-2</i>	<b>4</b>	100	31820	130000	1.68	77
13	<i>exo-2</i>	<b>3</b>	10	3182	36000	1.25	35
14	<i>exo-2</i>	<b>3</b>	30	9546	44000	1.50	68
15	<i>exo-2</i>	<b>3</b>	50	15910	59000	1.56	61
16	<i>exo-2</i>	<b>3</b>	70	22274	74000	1.55	74
17	<i>exo-2</i>	<b>3</b>	100	31820	106000	1.49	73

[a] Without end groups.

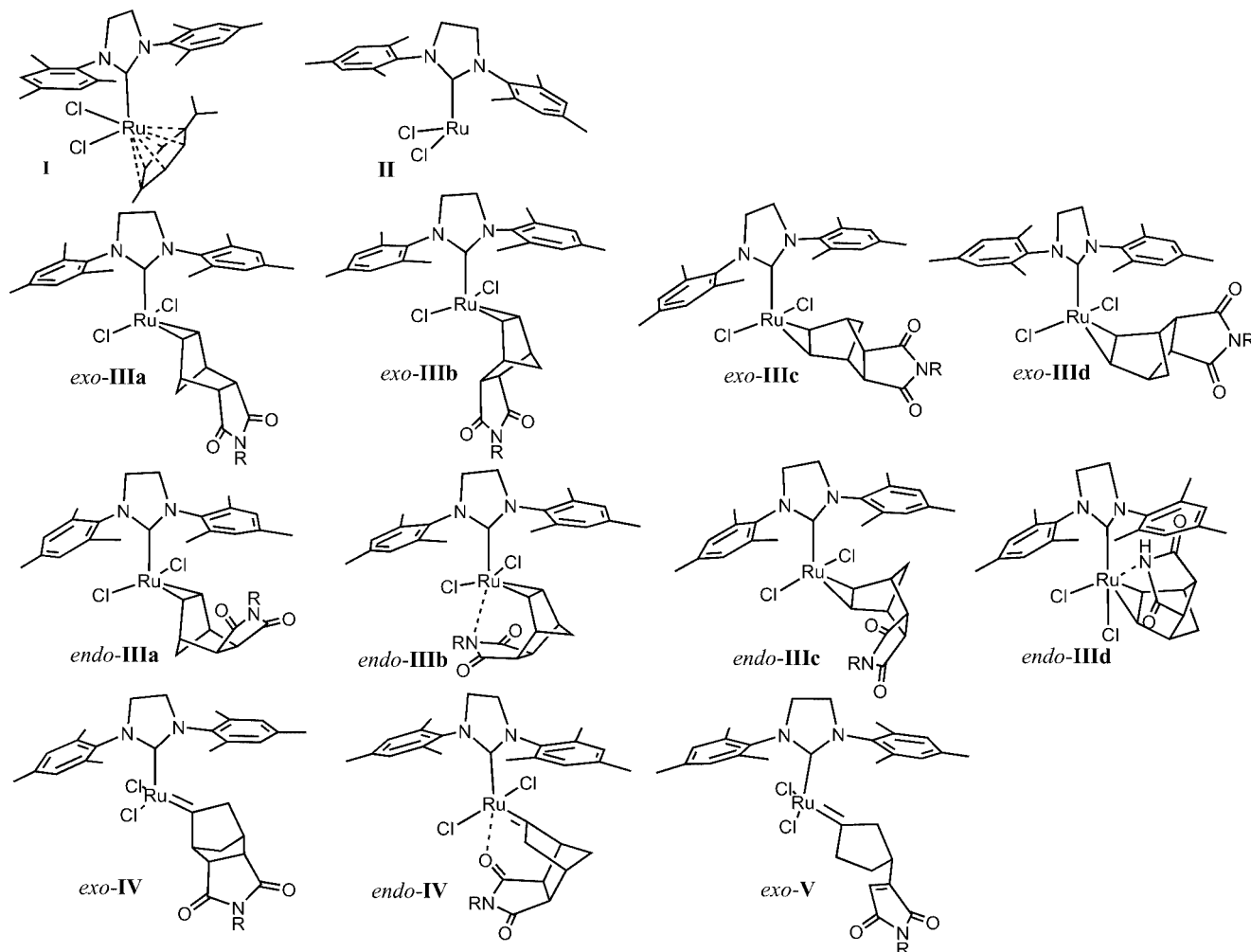


Figure 8. Structures of the studied complexes for the reaction of the *exo* and *endo* isomers with  $\text{RuCl}_2(\text{IMesH}_2)(p\text{-cymene})$ .

to form a 1,3-dimesityl-3,4-dihydroimidazolin-2-ylidene-based propagating species. These types of initiators have been reported to be far more active than the corresponding 1,3-dimesitylimidazol-2-ylidene-derived ones.<sup>[30]</sup> An important finding is the fact that the parent complex **5** is virtually inactive in the ROMP of *exo-1*, *endo-1*, *exo-2*, and *endo-2*. Thus, the exchange of both chlorine ligands by trifluoroacetates appears to be a necessary prerequisite for the formation of an active precatalyst. Similar behavior has been observed in the Ru-alkylidene-initiated cyclopolymerization of 1,6-heptadiynes, where substitution of both chlorines of the Grubbs<sup>[24]</sup> and Grubbs-Hoveyda-type initiators<sup>[21–23,31]</sup> by trifluoroacetate groups was necessary to generate polymerization-active systems. Precatalysts **6** and **6a**, as well as **7**, apparently decompose upon heating the polymerization mixture prior to any initiation. Finally, both precatalysts **8** and **9** are composed upon heating in the presence of any monomer. We tentatively assign this finding to an imine-type metathesis-type reaction<sup>[32,33]</sup> of dissociated phenylisonitrile with any in situ formed Ru-alkylidene complex resulting in cleavage of the Ru moiety from the polymer chain.

Polymerization results similar to those obtained for *endo-1* were observed for *exo-1*. Again, precatalyst **3** turned out to be more reactive than **4**. The values for  $M_n$  of poly(*exo-1*) as determined by LS (Table 1, entries 19 and 20) were significantly lower than those for poly(*endo-1*) (Table 1, entries 8 and 10), indicative of a higher initiation efficiency of the precatalyst for the *exo* monomer. Such higher reactivity of *exo* isomers versus Grubbs-type initiators was also reported by other groups.<sup>[34]</sup> In contrast to *endo-1*, polymerization of *endo-2* with either **3** or **4** resulted only in oligomeric or insoluble products that were isolated in low yields, typically <20% (Table 2, entries 1–7).

However, *exo-2* may be polymerized by both precatalysts **3** and **4** in a controlled way (Table 2, entries 8–17). PDIs were in the range of 1.69–2.05 for precatalyst **4** and 1.25–1.56 for precatalyst **3**. An illustration is given in Figure 8.

## Polymer Structure

The structure of poly(*endo-1*) prepared by the action of either **3** or **4** was identical to the one published previously.<sup>[35]</sup> An atactic, all-*trans* structure was assigned to this polymer. In contrast to poly(*endo-1*), poly(*exo-1*) and poly(*exo-2*), whether prepared by the action of **3** or **4**, showed a *cis* content of roughly 40%, as evidenced by signals in the <sup>1</sup>H NMR at  $\delta = 5.44$  ppm and in the <sup>13</sup>C NMR spectrum around  $\delta = 132$  ppm and 52 ppm, respectively. For NMR assignment of signals, see refs.<sup>[36–38]</sup>

## Theoretical Considerations

Quantum chemical calculations were carried out to shed some light on the possible mechanism of the formation of ROMP-active Ru-alkylidene complexes and to provide an explanation for the different reactivity of the *exo* and *endo*

forms of *N,N*-(norborn-5-ene-2,3-dicarbimide)-L-valine ethyl ester (NB-R1) and *N,N*-(norborn-5-ene-2,3-dicarbimide)-L-valine-*tert*-butylamide (NB-R2). For these calculations, the catalyst RuCl<sub>2</sub>(IMesH<sub>2</sub>)(*p*-cymene) was chosen as a model compound. Calculations revealed that the *exo* forms of both monomers studied are only insignificantly more stable (<2 kcal/mol) than the corresponding *endo* forms. Additionally, there is no essential effect of the substituent R {H, CH<sub>3</sub>, 2-propyl, CH[CH(CH<sub>3</sub>)<sub>2</sub>]COOEt, CH[CH(CH<sub>3</sub>)<sub>2</sub>]CONH-*t*Bu} and conformation (*exo* vs. *endo*) on the Mulliken atomic charges and electron density at the C=C double bond of monomers. Thus, the calculated Mulliken atomic charges at the C atoms forming the double bond are –0.106/–0.104 and –0.119/–0.118 for the *exo* and *endo* forms, respectively (R = CH<sub>3</sub>/R = H). Additionally, the calculated relative energies of the different Ru-alkylidene complexes for NB-R1 {R = CH[CH(CH<sub>3</sub>)<sub>2</sub>]COOEt} differ only slightly (<1 kcal/mol) from those calculated for R = H and CH<sub>3</sub>. Therefore, a simplified form of the monomers with R = H, which is not too time-consuming in frequency analysis, was used for further calculations.

After dissociation of the *p*-cymene ligand ( $\Delta U_{\text{tot}} = 6.2$  kcal/mol), the formation of the corresponding Ru-alkylidene complexes was calculated. In the case of the *exo*-form, four possible stable structures for the catalyst–monomer complexes (*exo-IIIa*, *exo-IIIb*, *exo-IIIc*, and *exo-IIId*) (Figure 8) were optimized, with *exo-IIIa* with C7 in proximity to the Ru center being the most stable one.

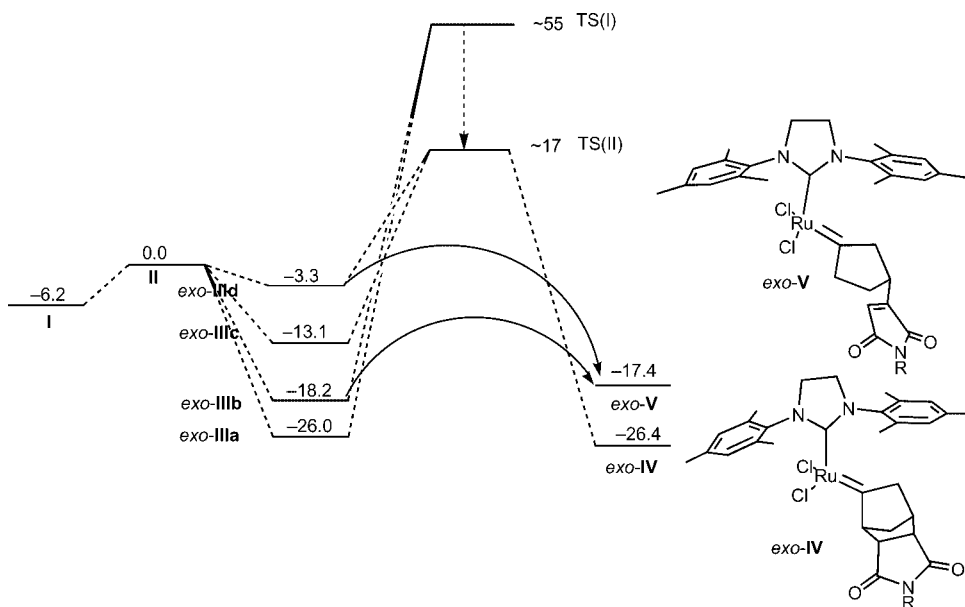
Complexes *exo-IIIa* and *exo-IIIb* are characterized by monomer C=C double bonds orthogonal to the Ru–NHC bond. In contrast, the C=C double bond in *exo-IIIc* and *exo-IIId* (Figure 8) is almost parallel to the Ru–NHC bond. The calculated relative stabilities of different structures are given in Table 3.

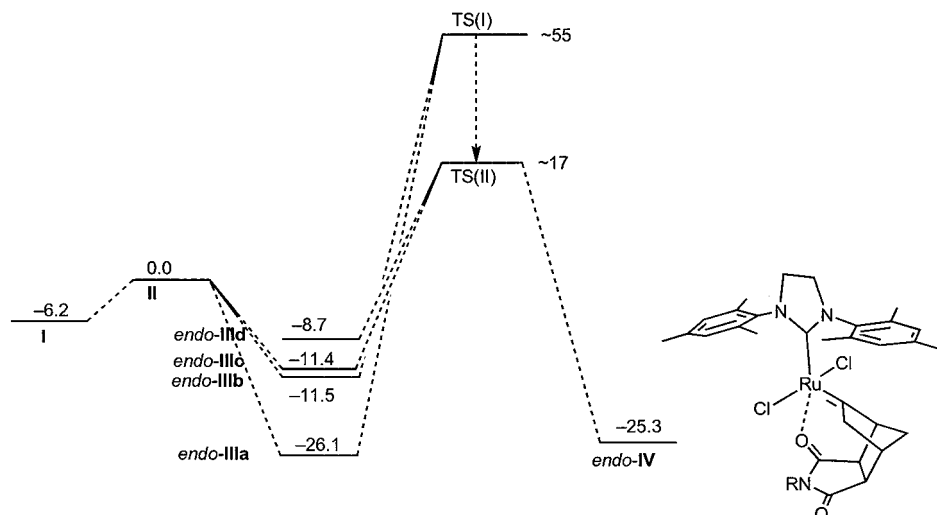
All four *exo*-monomer–Ru complexes are stable ( $\Delta U_{\text{tot}}$  is negative) and their possible transformations were further analyzed (Scheme 1).

Similar to the *exo* form, two stable catalyst–*endo*-monomer complexes with the C=C double bond of the monomer orthogonal to the Ru–NHC bond (*endo-IIIa* and *endo-IIIb*, Figure 8) were identified, *endo-IIIa* with C7 in proximity to the Ru center being the most stable one (Scheme 2). In addition, two structures, that is, *endo-IIIc* and *endo-IIId* with the C=C double bond of the monomer almost parallel to the Ru–NHC bond, are stable. Because of a strong steric interaction with the norborn-2-ene moiety, the Cl atom is *trans* to the N-heterocyclic carbene in *endo-IIId*. The calculated relative stabilities of the Ru–*endo*-monomer complexes (Table 3) indicate that formation of the structures *endo-IIIa*, *endo-IIIb*, *endo-IIIc*, and *endo-IIId* is exothermic ( $\Delta U_{\text{tot}}$  is negative) and their possible transformations were therefore further analyzed (Scheme 2). In addition, it could be argued that the existence of an additional interaction between Ru and the N atom of the monomer in the case of the *endo* form (structure *endo-IIIb*, Figure 8, Ru–N = 0.2407 nm) may prevent further transformation. Here the question arose whether an additional interaction between the Ru and the N atoms of the monomer calculated for the cut-down

Table 3. Relative energies [kcal/mol] of the different Ru complexes and activation energies  $U_{\text{act}}(E_0 + E_{\text{ZP}})$  [kcal/mol] for intramolecular C1–C2 H-shift.  $U_{\text{act}}$  was estimated for a simplified structure of the NHC (Supporting Information).

	Structure <i>exo</i>	Relative energy	Structure <i>endo</i>	Relative energy
$\Delta E_0$	<b>I</b>	-8.73	<b>I</b>	-8.73
$\Delta U_{\text{tot}}(E_0 + E_{\text{ZP}})$		-6.24		-6.24
$\Delta G_{\text{tot}}(U_{\text{tot}} - TS)$		9.71		9.71
$\Delta E_0$	<b>II</b>	0	<b>II</b>	0
$\Delta U_{\text{tot}}(E_0 + E_{\text{ZP}})$		0		0
$\Delta G_{\text{tot}}(U_{\text{tot}} - TS)$		0		0
$\Delta E_0$	<i>exo-IIIa</i>	-28.4	<i>endo-IIIa</i>	-28.44
$\Delta U_{\text{tot}}(E_0 + E_{\text{ZP}})$		-26.00		-26.05
$\Delta G_{\text{tot}}(U_{\text{tot}} - TS)$		-11.85		-11.31
$\Delta E_0$	<i>exo-IIIb</i>	-20.05	<i>endo-IIIb</i>	-13.82
$\Delta U_{\text{tot}}(E_0 + E_{\text{ZP}})$		-18.24		-11.53
$\Delta G_{\text{tot}}(U_{\text{tot}} - TS)$		-3.55		+5.19
$\Delta E_0$	<i>exo-IIIc</i>	-15.64	<i>endo-IIIc</i>	-13.76
$\Delta U_{\text{tot}}(E_0 + E_{\text{ZP}})$		-13.11		-11.46
$\Delta G_{\text{tot}}(U_{\text{tot}} - TS)$		+2.42		+3.40
$\Delta E_0$	<i>exo-IIId</i>	-5.45	<i>endo-IIId</i>	-9.1
$\Delta U_{\text{tot}}(E_0 + E_{\text{ZP}})$		-3.27		-7.0
$\Delta G_{\text{tot}}(U_{\text{tot}} - TS)$		+12.02		+11.2
$\Delta E_0$	<i>exo-IV</i>	-28.38	<i>endo-IV</i>	-27.25
$\Delta U_{\text{tot}}(E_0 + E_{\text{ZP}})$		-26.40		-25.33
$\Delta G_{\text{tot}}(U_{\text{tot}} - TS)$		-12.78		-9.02
$\Delta E_0$	<i>exo-V</i>	-17.96		
$\Delta U_{\text{tot}}(E_0 + E_{\text{ZP}})$		-17.36		
$\Delta G_{\text{tot}}(U_{\text{tot}} - TS)$		-4.33		
$U_{\text{act}}(E_0 + E_{\text{ZP}})$	TS(I) <i>exo-3a</i> → <b>4</b>	73	TS(I) <i>endo-3a</i> → <b>4</b>	74
$U_{\text{act}}(E_0 + E_{\text{ZP}})$	TS(II) <i>exo-3a</i> → <b>4</b>	41	TS(II) <i>endo-3a</i> → <b>4</b>	46
$U_{\text{act}}(E_0 + E_{\text{ZP}})$	TS(I) <i>exo-3b</i> → <b>4</b>	67	TS(I) <i>endo-3b</i> → <b>4</b>	–
$U_{\text{act}}(E_0 + E_{\text{ZP}})$	TS(II) <i>exo-3b</i> → <b>4</b>	33	TS(II) <i>endo-3b</i> → <b>4</b>	38
$U_{\text{act}}(E_0 + E_{\text{ZP}})$	TS(II) <i>exo-3c</i> → <b>4</b>	28	TS(II) <i>endo-3c</i> → <b>4</b>	34
$U_{\text{act}}(E_0 + E_{\text{ZP}})$	TS(II) <i>exo-3d</i> → <b>4</b>	18	TS(II) <i>endo-3d</i> → <b>4</b>	36

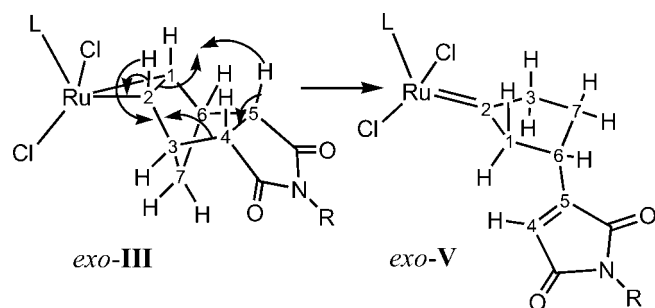
Scheme 1. Energy diagram and two possible reaction pathways calculated at the B3LYP/LACVP\* level for the reaction of an *exo* isomer with  $\text{RuCl}_2(\text{IMesH}_2)(p\text{-cymene})$ . Transition-state energies TS(I) and TS(II) are estimated for a simplified structure of the NHC (Supporting Information).



Scheme 2. Energy diagram and possible reaction pathways calculated at the B3LYP/LACVP\* level for the reaction of an *endo* isomer with  $\text{RuCl}_2(\text{IMesH}_2)(p\text{-cymene})$ . Transition-state energies TS(I) and TS(II) are estimated for a simplified structure of the NHC (Supporting Information).

model *N*-R-norborn-5-ene-2,3-dicarboximide ( $\text{R} = \text{H}, \text{CH}_3$ ) existed also for the actual monomers  $\{\text{R} = \text{CH}[\text{CH}(\text{CH}_3)_2]\text{-COOEt}, \text{CH}[\text{CH}(\text{CH}_3)_2]\text{CONH-}i\text{Bu}\}$  or whether other steric effects would dominate. To shed light on this point, calculations were carried out on the unrestricted monomers NB-R1 and NB-R2. As a matter of fact, these not only confirmed that this extra interaction exists, but revealed that the oxygen atom from the 2,3-dicarbimide group interacts very strongly with the Ru atom, thus forming an additional O–Ru bond. In due consequence, these two additional N–Ru and O–Ru interactions should aggravate any further transformation of *endo-IIIb* and thus further explain the reduced reactivity of the *endo*-monomer. The calculated *endo-IIIb* structures for NB-R1 and NB-R2 are given in Figure S2 in the Supporting Information.

To form the ROMP-active Ru–alkylidene complexes, the following mechanism may be proposed: one H atom from the  $\text{C1}=\text{C2}$  double bond shifts from C1 to C2 followed by formation of the Ru–alkylidene complex, leading to structures *exo-IV* or *endo-IV* (Schemes 2 and 3).



Scheme 3. Proposed reaction cascade for the formation of a ROMP-active  $\text{Ru}^{\text{IV}}$  alkylidene (structure *exo-5*).

Though structures *exo-IV* and *endo-IV* are energetically possible, the intramolecular  $\text{C1} \rightarrow \text{C2}$  H-shift proceeds with a high activation barrier and should therefore be analyzed. However, in contrast to stable structures, the optimization of transition states for such large molecules is comparably complicated. So, we were forced to use simplified molecular structures for the estimation of the barrier for possible models of intramolecular H-shifts. Thus, in the search of the transition state for the H-shift from C1 to C2 of the double bond we started from the corresponding *exo* and *endo* monomers (i.e., *exo*- and *endo-N*-R-norborn-5-ene-2,3-dicarboximide, respectively;  $\text{R} = \text{H}, \text{CH}_3$ ) not bonded to the Ru moiety. We found no effect of the substituents R on the nitrogen of the monomer on the structure and activation energy for the H-shift from C1 to C2. The calculated activation energy was very high (73 kcal/mol, 70 kcal/mol with Zero Point Energy correction). Transition structures of the monomer obtained that way were used as initial transition structures for the modeling of the different Ru–monomer complexes. A simplified catalyst structure with N–H instead of *N*-mesityl substituents was used.

Starting from the stable structures *exo-3a* and *exo-3b* (Scheme S1, Supporting Information), the transition structures [TS(I)] for the H-shift from C1 to C2 could be localized. The activation energy (given in Table 3) was again, as in the case of the nonbonded monomer, comparably high (up to 73 kcal/mol). However, when the H-shift from C1 to C2 was in conjunction with a concomitant formation of a Ru–alkylidene complex [TS(II)], the activation energy was essentially reduced, to 41 kcal/mol and 33 kcal/mol for *exo-3a* and *exo-3b*, respectively. Starting from the stable structures *exo-3c* and *exo-3d* (Scheme S1, Supporting Information), the transition structures [TS(I)] could not be localized and transformed directly into the corresponding sec-

ond transition structures [TS(II)]. This is a consequence of the geometries of TS(II), which have the alkylidene parallel to the Ru–NHC bond and do not need any additional rotation of the ruthenacyclopropane ring as is the case in *exo-3a* and *exo-3b*. Vice versa, the ruthenacyclopropane rings in *exo-3c* and *exo-3d* also already occupy a parallel orientation with respect to the Ru–NHC bond. The analysis of the TS(II) structures showed that in the case of the *exo* form only two structures of the TS(II) with very small differences in energy ( $<1$  kcal/mol) exist. Here, the *exo-3a* structure is identical to *exo-3c* and *exo-3b* is identical to *exo-3d* (Supporting Information).

Starting from the stable structure *endo-3a* (Scheme S2, Supporting Information), the transition structure [TS(I)] for the H-shift from C1 to C2 could be localized with a very high activation energy (74 kcal/mol). In case the H-shift occurs concomitantly to a rotation of the ruthenacyclobutane, formation of a Ru–alkylidene complex occurs, and the activation energy is again essentially reduced to 46 kcal/mol [TS(II)] (Scheme S2, Supporting Information). TS(I) could not be localized for *endo-3b*, *endo-3c*, and *endo-3d* and transformed directly into the second transition structure [TS(II)]. Again, the TS(II) of *endo-3a* is identical to that of *endo-3c*. Formation of the TS(II) of *endo-3b*, being identical to that of *endo-3d*, was calculated to be slightly more favorable (about 2 kcal/mol) than the TS(II) of *endo-3a* and *endo-3c*.

Activation energies for the intramolecular C1  $\rightarrow$  C2 H-shift were calculated for the simplified structure of the NHC ligand with N–H instead of *N*-mesityl groups. These were further used for the analysis of the possible transformations of the Ru–alkylidene complexes (Table 3). However, it should be noted that the calculated activation energies for the 1,2-H-shift for the simplified form of the monomer (R = H) should be used on a qualitative rather than on a quantitative base. From the analysis of the data summarized in Table 3 it can be seen that the formation of TS(II) is particularly favorable (18 kcal/mol) in case the reaction proceeds via the *exo-IIIId* structure.

From the analysis of the formation of the ROMP-active structures *exo-IV* and *endo-IV* through C<sub>1</sub>  $\rightarrow$  C<sub>2</sub> H-shift (Schemes 1 and 2) follows: (i) the ROMP-active structure *exo-IV* can be built starting from all four stable structures *exo-IIIa*, *exo-IIIb*, *exo-IIIc*, and *exo-IIId*; its formation is energetically favorable ( $\Delta U_{\text{tot}} = -26.0$  kcal/mol,  $-18.2$  kcal/mol,  $-13.1$  kcal/mol, and  $-3.3$  kcal/mol, respectively); (ii) the transformation starting from the less stable complex *exo-IIId* occurs with lower activation energy (only 18 kcal/mol) than from the most stable structure *exo-IIIa*, indicating a low-energy pathway; (iii) the formation of *endo-IV* by the low-energy pathway starting from the less stable structure *endo-IIIc* occurs with activation energy 31 kcal/mol, which is 13 kcal/mol higher than that for the pathway starting from *exo-IIId*. Moreover, the structure *endo-IIIb* seems to be inactive because of additional Ru–N bonding. Finally, the structure *endo-IV* must be further expected to be virtually ROMP-inactive because of the formation of an additional Ru–O bond (Scheme 2, bond length = 0.240 nm).

All these findings may be indicative of a lower activity of the *endo* forms of the monomers investigated in comparison to the corresponding *exo* forms.

An additional, alternative *activation mechanism* for the formation of Ru–alkylidene complexes necessary for ROMP may explain the different reactivity of the *exo* and *endo* forms of **1** and **2**. While there is no essential difference between the *exo* and *endo* forms of monomers in the electronic parameters, such as charge and electron density at the double bond, there is a deciding contrast in geometry. As can be seen in Figure 9, there is a significant difference in the distances between the C1 atom of the double bond and the H5 atom at the *exo* or *endo* position (0.269 nm and 0.367 nm, for *exo* or *endo* respectively).

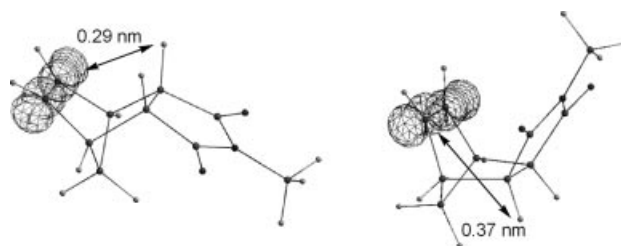
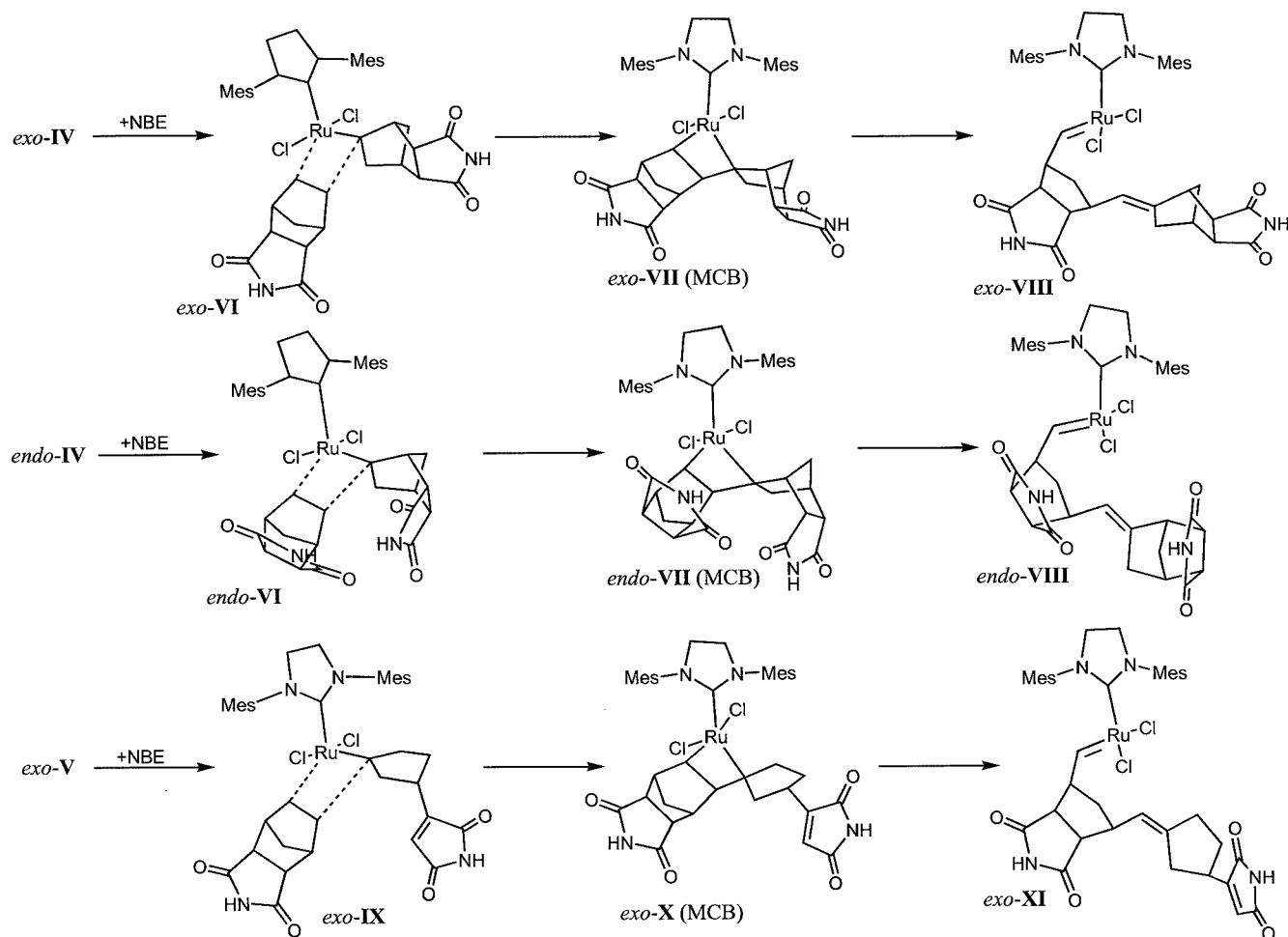


Figure 9. Distances between C1/C2 atoms of the double bond (the  $p_z$  orbitals) and the H atoms at C4/C5 in the *exo* and *endo* forms.

Consequently, the positively charged H atom in the *exo* position interacts strongly with the  $p_z$  orbital on the negatively polarized C1, thus facilitating the intramolecular C5  $\rightarrow$  C1 (or C4  $\rightarrow$  C2) H-shift to the double bond. As geometry optimization reveals, the weakening of the C3–C4 bond could be followed by ring opening, concomitant intramolecular H-shift from C2 to C1, and formation of a Ru=C double bond. All these intramolecular transformations can apparently occur concomitantly (Scheme 3) with low activation energies leading to the structure *exo-V*. However, such transformation is impossible in the case of the *endo* form. For this reaction pathway, the starting complexes *exo-IIIb* and especially *exo-IIId* appear to be more favorable than complexes *exo-IIIa* and *exo-IIIc* for two reasons. First, as a consequence of the interaction between the double bond and the Ru center, the geometry on C1 and C2 is no longer planar (there is some admixture of  $sp^3$  hybridization), thus leading to the deformation of  $p_z$  electron density from the C atoms in the direction of the H atom at C4 and C5, respectively. This facilitates the interaction with the H atom and consequently the H-shift. This also explains the stability of the monomer in the absence of any catalyst. Second, as revealed by calculations, complexes *exo-IIIb* and *exo-IIId* are also energetically favorable for transformation into the activated catalyst *exo-V* ( $\Delta G_{\text{tot}} = -0.8$  kcal/mol and  $\Delta G_{\text{tot}} = -16.35$  kcal/mol respectively).

It should be emphasized that so far the discussed mechanism through the possible H-shift from C4 to C2 is only *qualitative* because of computational restrictions in the search for transition structures that operate through a concerted transformation (H-shifts and ring opening). However, such transformations are expected to occur easily be-



Scheme 4. Most stable structures of Ru-alkylidene complexes (B3LYP/LACVP\*).

cause of a favorable geometry for the H-shift in the *exo-IIIb* and *exo-IIIc* complexes and the better interaction of the proton with the  $p_z$  electrons of the double bond.

The mechanism discussed so far for the formation of Ru-alkylidene complexes (structures *exo-IV*, *exo-V*, and *endo-IV*) necessary for ROMP clearly shows the difference between the *exo* and *endo* forms. However, it might be of interest to identify the rate-determining step of the overall polymerization reaction. To understand differences in reactivities of the *exo* and *endo* forms, further insertion reactions of a second norborn-2-ene monomer into *exo-IV*, *exo-V*, and *endo-IV* were calculated. The calculated structures are shown in Scheme 4.

It was found that both active complexes *exo-IV* and *endo-IV* form stable  $\pi$  complexes (structures *exo-VI* and *endo-VI*) with stabilization energies of 2.6 kcal/mol and 0.6 kcal/mol respectively. The active complex *exo-V* can form a stable  $\pi$  complex (*exo-IX*) with norborn-2-ene (stabilization energy 3.1 kcal/mol) too. However, the next steps, that is, the conversion of the  $\pi$  complex into the corresponding metallacyclobutane (MCB) structures *exo-VII* (MCB), *exo-X* (MCB), and *endo-VII* (MCB) (Scheme 4) followed by ring opening (structures *exo-VIII*, *exo-XI*, and *endo-VIII*), proceed energetically differently for the *exo* and

*endo* forms. Thus, though the ring-opening reaction is energetically favorable in all three cases, the formation of the MCB structure is very different for *exo* and *endo* forms. In the cases of *exo-IV* and *exo-V*, stable structures of the MCB were calculated with reaction enthalpies around  $-1.0$  kcal/mol and  $-2.5$  kcal/mol for *exo-VII* (MCB) and *exo-X* (MCB) respectively. On the contrary, *endo-VII* (MCB) is only a transition structure requiring an activation energy for MCB formation of about 17 kcal/mol. Such different behavior of the *endo* form is apparently caused by a strong steric interaction of the Cl ligand with the substituents at the *N*-imido group. In due consequence, the large activation energy for the MCB formation in the case of the *endo* form may be the rate-determining step of the overall polymerization reaction. A comprehensive study on the different reactivity of various *exo*- and *endo*-norborn-5-ene-2,3-dicarbimides is now in progress.

## Conclusions

A series of novel Ru<sup>II</sup>-derived precatalysts have been investigated for their polymerization behavior in the ROMP of *exo*- and *endo*-norborn-5-ene-2,3-dicarbimides. Our in-

vestigations revealed that precatalysts containing an N-heterocyclic carbene ligand, two trifluoroacetate groups, and one labile ligand are best suited for the thermal initiation of ROMP. The *exo* isomer was preferentially polymerized in both cases. Quantum chemical calculations propose possible mechanisms for the formation of ROMP-active structures, which could also explain the experimental findings of the better reactivity of the *exo* form. Additionally, the different activation energies for MCB formation of the *exo* and *endo* forms may be the rate-determining step of the overall polymerization reaction. Further work will focus on the construction of suitable labile ligands that allow for a *quantitative initiation* of the precatalysts.

## Experimental Section

All manipulations were performed under nitrogen in a glovebox (MBraun LabMaster 130) or by standard Schlenk techniques. Purchased starting materials were used without any further purification. Dichloroethane was distilled from calcium hydride under nitrogen. Tetrahydrofuran (THF), pentane, diethyl ether, toluene, and dichloromethane were dried by an MBraun solvent purification system (SPS). NMR spectroscopic data were obtained at 250.13 MHz for proton and 62.90 MHz for carbon in the indicated solvent at 25 °C on a Bruker Spectrospin 250 and are listed in parts per million downfield from tetramethylsilane for proton and carbon. IR spectra were recorded with a Bruker Vector 22 using ATR technology. Molecular weights and polydispersity indices (PDIs) of the polymers were determined by GPC at 30 °C on Polymer laboratories columns (PLgel 10 µm MIXED-B, 7.5 × 300 mm) in THF at 25 °C using a Waters Autosampler, a Waters 484 UV spectrometer detector (254 nm), an Optilab Rex refractive index detector (Wyatt), and a MiniDawn light-scattering detector (Wyatt). Synthesis and structural data of compounds *endo-1* and *endo-2*,<sup>[28]</sup> **3**, **4**, **9**, **10**,<sup>[14]</sup> and **5**<sup>[6]</sup> have been reported elsewhere. Values for *dn/dc* for *endo-1*, *exo-1*, and *exo-2* were 0.119, 0.126, and 0.116, respectively.

**exo,exo-N,N-(Norborn-5-ene-2,3-dicarbimido)-L-valine Ethyl Ester (*exo-1*):** *exo,exo-N,N*-(Norborn-5-ene-2,3-dicarbimido)-L-valine (575 mg, 2.18 mmol) and *p*-toluenesulfonic acid (17 mg, 0.08 mmol) were dissolved in dry ethanol and refluxed for 8 h. The ethanol was evaporated and the residue was dissolved in diethyl ether. The ether solution was subject to flash chromatography over silica gel 60 (diethyl ether/pentane, 5:1). Recrystallization gave *exo-1* as white needles in 35% yield (220 mg). IR (ATR):  $\tilde{\nu}$  = 2975 (w), 1739 (m), 1693 (s), 1526 (m), 1380 (s), 1352 (m), 1281 (w), 1186 (s), 1097 (m), 1050 (m), 1018 (m), 969 (m), 892 (m), 825 (m), 771 (m), 724 (w), 673 (m) cm<sup>-1</sup>. <sup>1</sup>H NMR (CDCl<sub>3</sub>):  $\delta$  = 6.30 (s, 2 H), 4.34 (d, <sup>1</sup>J = 8.1 Hz, 1 H), 4.25–4.08 (m, 2 H), 3.31 (br. s, 2 H), 2.78–2.57 (m, 3 H), 1.53 (m, 2 H), 1.20 (t, <sup>2</sup>J = 7.17 Hz, 3 H, CH<sub>3</sub>), 1.10 (d, <sup>2</sup>J = 6.67 Hz, 3 H, CH<sub>3</sub>), 0.84 (d, <sup>2</sup>J = 6.84 Hz, 3 H, CH<sub>3</sub>) ppm. <sup>13</sup>C NMR (CDCl<sub>3</sub>):  $\delta$  = 177.4, 177.26, 168.3, 137.9, 61.37, 57.7, 47.8, 47.3, 45.6, 45.37, 42.8, 27.9, 22.3, 21.03, 19.34, 14.01 ppm. MS: calcd. for C<sub>16</sub>H<sub>21</sub>NO<sub>4</sub> [M]<sup>+</sup> 291.15; found 291.

**exo,exo-N,N-(Norborn-5-ene-2,3-dicarbimido)-L-valine-tert-butylamide (*exo-2*):** Dicyclohexyldicarbodiimide (DCC, 1.96 g, 0.95 mmol) was added to L-valine-*exo,exo-N,N*-(norborn-2-ene-5,6-dicarbimide) (5.0 g, 1.9 mmol) dissolved in acetonitrile. Soon after addition of DCC, dicyclohexylurea (DCU) precipitated, and the reaction mixture was stirred for a further 6 h. DCU was filtered off, *tert*-butylamine (2.0 mL, 1.9 mmol) was added to the filtrate,

and the reaction mixture was stirred for 12 h. Finally, the ammonium salt was filtered off. Acetonitrile was evaporated under reduced pressure until an oily residue remained, which was dissolved in diethyl ether. The ether solution was subsequently washed with 0.1 M hydrochloric acid and saturated aqueous sodium hydrogen carbonate and finally dried with sodium sulfate. The solution was concentrated, and about the same amount of pentane was added. Crystallization was performed at –18 °C. Yield: 2.6 g (43%). IR (ATR-mode):  $\tilde{\nu}$  = 3353 (m), 2965 (w), 2929 (m), 2864 (m), 1690 (s), 1523 (m), 1454 (m), 1376 (s), 1352 (s), 1212 (w), 1182 (s), 1044 (m), 927 (m), 891 (m), 858 (m), 823 (m), 777 (m), 720 (w) cm<sup>-1</sup>. <sup>1</sup>H NMR (CDCl<sub>3</sub>):  $\delta$  = 6.63 (br. s, 1 H, NH), 6.11 (m, 2 H), 3.94 (d, <sup>2</sup>J = 11.54 Hz, 1 H, CH), 3.42 (br., 2 H), 3.29 (m, 2 H), 2.60 (m, 1 H), 1.74 (d, <sup>1</sup>J = 8.8 Hz, 1 H), 1.54 (d, <sup>1</sup>J = 8.9 Hz, 1 H), 1.30 (s, 9 H, *t*Bu), 0.98 (d, <sup>2</sup>J = 6.67 Hz, 3 H, CH<sub>3</sub>), 0.75 (d, <sup>2</sup>J = 6.52 Hz, 3 H, CH<sub>3</sub>) ppm. <sup>13</sup>C NMR (CDCl<sub>3</sub>):  $\delta$  = 178.31, 177.83, 167.50, 134.89, 134.6, 65.03, 52.35, 51.03, 45.58, 45.41, 45.12, 28.53, 26.50, 19.54 ppm. MS: calcd. for C<sub>18</sub>H<sub>26</sub>N<sub>2</sub>O<sub>3</sub> [M]<sup>+</sup> 318.19; found 276 [M – H<sub>3</sub>C–CH=CH<sub>2</sub>]<sup>+</sup>.

**[Ru(CF<sub>3</sub>CO<sub>2</sub>)(*p*-cymene)PCy<sub>3</sub>] (6):** [RuCl<sub>2</sub>(*p*-cymene)]<sub>2</sub><sup>[39]</sup> was treated with 2 equiv. of PCy<sub>3</sub> and [RuCl<sub>2</sub>(*p*-cymene)PCy<sub>3</sub>] was obtained in 90% yield according to ref.<sup>[5]</sup> <sup>1</sup>H NMR (CDCl<sub>3</sub>):  $\delta$  = 5.58 (br. s, 4 H, ArH), 2.83 [pent, <sup>2</sup>J = 6.9 Hz, 1 H, CH(CH<sub>3</sub>)<sub>2</sub>], 2.42 (q, *J* = 22.3, 11.4 Hz, 3 H, cyclohexyl), 2.14 (s, 3 H, CH<sub>3</sub>), 2.09 (br., 6 H, cyclohexyl), 1.88–1.66 (m, 9 H, cyclohexyl), 1.30 [d, <sup>2</sup>J = 7.0 Hz, 6 H, CH(CH<sub>3</sub>)<sub>2</sub>], 1.56–1.10 (m, 15 H, cyclohexyl) ppm. <sup>13</sup>C NMR (CDCl<sub>3</sub>):  $\delta$  = 106.7, 94.2, 88.2 (*J*<sub>31P-13C</sub> = 3.8 Hz), 83.7 (*J*<sub>31P-13C</sub> = 4.9 Hz), 35.7 (*J*<sub>31P-13C</sub> = 17.9 Hz, cyclohexyl), 30.4 (s, cyclohexyl), 29.5 (*J*<sub>31P-13C</sub> = 2.1 Hz, cyclohexyl), 27.4 (*J*<sub>31P-13C</sub> = 9.8 Hz, cyclohexyl), 26.3 [CH(CH<sub>3</sub>)<sub>2</sub>], 22.3 [CH(CH<sub>3</sub>)<sub>2</sub>], 17.7 (CH<sub>3</sub>) ppm.

[RuCl<sub>2</sub>(*p*-cymene)PCy<sub>3</sub>] (114 mg, 0.20 mmol) was dissolved in THF and added to a solution of silver trifluoroacetate (97.2 mg, 0.44 mmol) in THF, both cooled to –36 °C. After mixing, the solution was stirred for another 4 h, allowing it to reach room temperature. During that time a white precipitate of AgCl formed. The mixture was filtered through celite and the THF was removed in vacuo. Methylene chloride was added to dissolve the residue and the solution was again concentrated in vacuo. Diethyl ether and *n*-pentane were successfully layered over the red, saturated solution. Yield: 82%. FTIR (ATR mode):  $\tilde{\nu}$  = 2934, 2853, 2052, 1701, 1448, 1396, 1187, 1126, 1006, 837, 784, 725, 672 cm<sup>-1</sup>. <sup>1</sup>H NMR (CDCl<sub>3</sub>):  $\delta$  = 6.14 (d, <sup>2</sup>J = 5.9 Hz, 2 H, ArH), 6.14 (d, <sup>2</sup>J = 6.1 Hz, 2 H, ArH), 2.60 [pent, <sup>2</sup>J = 6.9 Hz, 1 H, CH(CH<sub>3</sub>)<sub>2</sub>], 2.25 (q, *J* = 11.9 Hz, 3 H, cyclohexyl), 2.07 (s, 3 H, CH<sub>3</sub>), 1.98–1.69 (m, 15 H, cyclohexyl), 1.56–1.22 (m, 15 H, cyclohexyl), 1.18 [d, <sup>2</sup>J = 6.9 Hz, 6 H, CH(CH<sub>3</sub>)<sub>2</sub>] ppm. <sup>13</sup>C NMR (CDCl<sub>3</sub>):  $\delta$  = 163.0 [dq, <sup>2</sup>J<sub>19F-13C</sub> = 36.3, 2.5 Hz, CO], 114.6 (q, <sup>1</sup>J<sub>19F-13C</sub> = 291.1 Hz, CF<sub>3</sub>), 107.2, 94.8, 84.2 (*J*<sub>31P-13C</sub> = 3.0 Hz), 81.8 (*J*<sub>31P-13C</sub> = 3.9 Hz), 35.6 (*J*<sub>31P-13C</sub> = 17.0 Hz, cyclohexyl), 31.5 (cyclohexyl), 29.3 (*J*<sub>31P-13C</sub> = 2.2 Hz, cyclohexyl), 27.7 (*J*<sub>31P-13C</sub> = 9.9 Hz, cyclohexyl), 26.4 [CH(CH<sub>3</sub>)<sub>2</sub>], 22.5 [CH(CH<sub>3</sub>)<sub>2</sub>], 18.8 (CH<sub>3</sub>) ppm. C<sub>32</sub>H<sub>47</sub>F<sub>6</sub>O<sub>4</sub>PRu (742.22): calcd. C 51.82, H 6.39; found C 51.87, H 6.50. Crystals of compound **6** were obtained in the form of its CF<sub>3</sub>COOAg adduct (**6a**).

**[Ru(CF<sub>3</sub>CO<sub>2</sub>)<sub>2</sub>(*p*-cymene)PPh<sub>3</sub>] (7):** [RuCl<sub>2</sub>(*p*-cymene)]<sub>2</sub> was treated with PPh<sub>3</sub> (2 equiv.) according to the literature to give [RuCl<sub>2</sub>(*p*-cymene)PPh<sub>3</sub>] in 98% yield.<sup>[33]</sup> <sup>1</sup>H NMR (CDCl<sub>3</sub>):  $\delta$  = 7.87–7.79 (m, 6 H, Ph), 7.40–7.32 (m, 9 H, Ph), 5.24 (d, <sup>2</sup>J = 6.2 Hz, 2 H, ArH), 4.98 (dd, <sup>2</sup>J = 6.2, 1.2 Hz, 2 H, ArH), 2.85 [pent, <sup>2</sup>J = 6.2 Hz, 1 H, CH(CH<sub>3</sub>)<sub>2</sub>], 1.86 (s, 3 H, CH<sub>3</sub>), 1.09 [d, <sup>2</sup>J = 6.2 Hz, 6 H, CH(CH<sub>3</sub>)<sub>2</sub>] ppm. <sup>13</sup>C NMR (CDCl<sub>3</sub>):  $\delta$  = 134.3 (<sup>2</sup>J<sub>31P-13C</sub> = 9.4 Hz, Ph), 133.7 (<sup>1</sup>J<sub>31P-13C</sub> = 45.7 Hz, Ph), 130.2 (<sup>4</sup>J<sub>31P-13C</sub> = 2.2 Hz, Ph),

127.9 ( $^2J_{31\text{P},13\text{C}} = 9.9$  Hz, Ph), 111.2 ( $^2J_{31\text{P},13\text{C}} = 3.3$  Hz, *p*-Cym), 95.9 (*p*-Cym), 89.0 ( $^2J_{31\text{P},13\text{C}} = 3.3$  Hz, *p*-Cym), 87.1 ( $^2J_{31\text{P},13\text{C}} = 3.3$  Hz, *p*-Cym), 30.2, 21.8, 17.7 (mesityl) ppm.

[RuCl<sub>2</sub>(*p*-cymene)PPh<sub>3</sub>] (56.8 mg, 0.10 mmol) was dissolved in THF and added to a solution of silver trifluoroacetate (44.2 mg, 0.20 mmol) in THF, both cooled to -36 °C. After mixing, the solution was stirred for another 4 h, allowing it to reach room temperature. During that time a white precipitate of AgCl formed. The mixture was filtered through celite and the THF was removed in vacuo. Methylene chloride was added to dissolve the residue and the solution was again concentrated in vacuo. Diethyl ether and *n*-pentane were successfully layered over the red, saturated solution. Red crystals formed at -36 °C. Yield: 62.2 mg, 86%. FTIR:  $\tilde{\nu} = 3057, 1679, 1436, 1405, 1183, 1139, 1095, 845, 788, 750, 694, 620$  cm<sup>-1</sup>. <sup>1</sup>H NMR (CDCl<sub>3</sub>):  $\delta = 7.51\text{--}7.43$  (m, 9 H, Ph), 7.40–7.34 (m, 6 H, Ph), 6.26 (d,  $^2J = 5.1$  Hz, 2 H, ArH), 4.98 (d,  $^2J = 5.1$  Hz, 2 H, ArH), 2.58 [pent,  $^2J = 6.9$  Hz, 1 H, CH(CH<sub>3</sub>)<sub>2</sub>], 1.68 (s, 3 H, CH<sub>3</sub>), 1.26 (d,  $^2J = 6.9$  Hz, 6 H, CH<sub>3</sub>) ppm. <sup>13</sup>C NMR (CDCl<sub>3</sub>):  $\delta = 163.6$  (dq,  $^2J_{19\text{F},13\text{C}} = 36.6, 1.8$  Hz, CO), 134.4 ( $^2J_{31\text{P},13\text{C}} = 10.4$  Hz, Ph), 130.9 ( $^4J_{31\text{P},13\text{C}} = 2.3$  Hz, Ph), 129.5 ( $^1J_{31\text{P},13\text{C}} = 47.2$  Hz, Ph), 128.4 ( $^3J_{31\text{P},13\text{C}} = 10.4$  Hz, Ph), 114.8 (q,  $^1J_{19\text{F},13\text{C}} = 291.1$  Hz, CF<sub>3</sub>), 115.2 ( $^2J_{31\text{P},13\text{C}} = 8.4$  Hz, *p*-Cym), 95.7 (*p*-Cym), 86.6, 86.5 ( $^2J_{31\text{P},13\text{C}} = 3.4$  Hz, *p*-Cym), 82.8 (*p*-Cym), 31.4 [CH(CH<sub>3</sub>)<sub>2</sub>], 21.8, 18.1 (CH<sub>3</sub>) ppm.

**Typical Procedure for ROMP:** Polymerizations were performed under argon. A solution of the corresponding initiator (5 mg) in ClCH<sub>2</sub>CH<sub>2</sub>Cl (1 mL) was added to a solution of the monomer in ClCH<sub>2</sub>CH<sub>2</sub>Cl (3 mL). The mixture was stirred at 70 °C for 8 h, then concentrated to about 1 mL, then the polymer was precipitated by dropwise addition of the solution to 30 mL of acidic methanol. The product was then filtered and dried in vacuo to give an off-white to light yellow powder.

**Poly(*exo*-1) Prepared by the Action of 3:**  $M_n = 88000$  g/mol;  $M_w = 209000$  g/mol; PDI = 2.36. IR (ATR):  $\tilde{\nu} = 2964, 1740, 1702, 1456, 1375, 1269, 1182, 1129, 1025, 968, 812, 650$  cm<sup>-1</sup>. <sup>1</sup>H NMR (CDCl<sub>3</sub>):  $\delta = 5.76$  (br. s), 5.44 (br. s), 4.28–4.16 (m, 3 H), 3.04 (m, 3 H), 2.62 (m, 2 H), 2.15 (m, 1 H), 1.62 (m, 1 H), 1.23 (t,  $^2J = 7.1$  Hz, 3 H), 1.10 (d,  $^2J = 6.5$  Hz, 3 H), 0.83 (d,  $^2J = 6.7$  Hz, 3 H) ppm. <sup>13</sup>C NMR (CDCl<sub>3</sub>):  $\delta = 177.6, 168.3, 132$  (unresolved m), 131.6, 61.3, 57.5, 52.0 (unresolved), 50.6, 45.9, 41.8, 27.7, 21.2, 19.3, 14.1 ppm. NMR spectra of poly(*exo*-1) prepared by the action of 4 ( $M_n = 130200$  g/mol;  $M_w = 225800$  g/mol; PDI = 1.73) were identical.

**Poly(*endo*-1) Prepared by the Action of 3:**  $M_n = 158300$  g/mol;  $M_w = 218900$  g/mol; PDI = 1.38. IR (ATR):  $\tilde{\nu} = 2967, 1739, 1700$  (s), 1461, 1380, 1274, 1188, 1133, 1028, 969, 922, 821, 715, 661 cm<sup>-1</sup>. <sup>1</sup>H NMR (CDCl<sub>3</sub>):  $\delta = 5.65$  (br. m, 2 H), 4.33 (m, 1 H), 4.14 (m, 2 H), 3.24 (br. s, 3 H), 2.93 (br. s, 1 H), 2.58 (br. s, 1 H), 1.86 (br. s, 1 H), 1.35–1.22 (m, 4 H), 1.08 (br. s, 3 H), 0.79 (br. s, 3 H) ppm. <sup>13</sup>C NMR (CDCl<sub>3</sub>):  $\delta = 176.1, 175.3, 168.3, 129.3, 61.4, 57.7, 48.4, 45.5, 40.3, 37.3$  (br), 27.5, 21.2, 19.4, 14.1 ppm. NMR spectra of poly(*endo*-1) prepared by the action of 4 ( $M_n = 90900$  g/mol;  $M_w = 125600$  g/mol; PDI = 1.39) were identical.

**Poly(*exo*-2) Prepared by the Action of 3:**  $M_n = 106000$  g/mol;  $M_w = 158000$  g/mol; PDI = 1.49. IR (ATR):  $\tilde{\nu} = 2963, 1772, 1697, 1536, 1455, 1360, 1183, 1131, 967, 650$  cm<sup>-1</sup>. <sup>1</sup>H NMR (CDCl<sub>3</sub>):  $\delta = 6.75$  (br. s), 5.75–5.48 (m), 4.05 (m, 1 H), 3.02 (br. s, 3 H), 2.68 (br. s, 2 H), 2.15 (br. s, 1 H), 1.62 (m, 1 H), 1.31 (s, 9 H), 1.03 (d,  $^2J = 6.24$  Hz, 3 H), 0.79 (d,  $^2J = 6.18$  Hz, 3 H) ppm. <sup>13</sup>C NMR (CDCl<sub>3</sub>):  $\delta = 178.4, 167.4, 132$  (unresolved m), 131.6, 64.8, 51.2 (unresolved), 50.4, 46.2, 41.8, 28.5, 26.7, 19.6, 19.3 ppm. NMR

spectra of poly(*exo*-2) prepared by the action of 4 ( $M_n = 130000$  g/mol;  $M_w = 218500$  g/mol; PDI = 1.68) were identical.

**Computational Methods:** Density Functional Theory (DFT) calculations were carried out using Becke's three-parameter functional (B3)<sup>[40,41]</sup> in combination with the Lee, Yang, and Parr (LYP) correlation functional<sup>[42]</sup> with the LACVP\* basis set (Jaguar, version 6.5 program<sup>[43]</sup>). The LACVP\* basis set uses the standard 6-31G\* basis set for light elements and the LAC pseudopotential<sup>[44]</sup> for the Ru atom. The molecular geometries and energies of all calculated structures were obtained at the same B3LYP/LACVP\* level of theory. The B3LYP/LACVP\* method has already been successfully used in many studies.<sup>[45–48]</sup> To prove the ability of this method, the calculated molecular structure of precatalyst 3 was compared with its X-ray structure.

The calculated parameters of structure 3 were in good agreement with those of the X-ray structure (given in Supporting Information Figure S1 and Table S1). Frequency analysis was used throughout for identification of the stationary points, which is especially important for the search of the transition states, and to obtain thermochemistry parameters such as zero point energy ( $E_{\text{ZP}}$ ), entropy ( $S$ ), total internal energy ( $U_{\text{tot}}$ ), total enthalpy ( $H_{\text{tot}}$ ), and total Gibbs free energy ( $G_{\text{tot}}$ ) at 298 K. The relative stability of the different structures was calculated as a balance of both  $U_{\text{tot}}$  and  $G_{\text{tot}}$  relative to those of the intermediary RuCl<sub>2</sub>(IMesH<sub>2</sub>) complex (structure II in Scheme 1).

#### X-ray Measurement and Structure Determination of 3, 6a, and 7–9:

Data collection was performed with a Nonius Kappa CCD equipped with graphite-monochromated Mo- $K_{\alpha}$  radiation ( $\lambda = 0.71073$  Å) and a nominal crystal-to-area detector distance of 36 mm. Intensities were integrated using DENZO and scaled with SCALEPACK.<sup>[49]</sup> Several scans in  $\phi$  and  $\omega$  directions were made to increase the number of redundant reflections, which were averaged in the refinement cycles. This procedure replaces in a good approximation an empirical absorption correction. The structures were solved with direct methods SHELXS86 and refined against  $F^2$  SHELXL97.<sup>[50]</sup> The function minimized was  $\sum[w(F_o^2 - F_c^2)^2]$  with the weight defined as  $w^{-1} = [\sigma^2(F_o^2) + (xP)^2 + yP]$  and  $P = (F_o^2 + 2F_c^2)/3$ . All non-hydrogen atoms were refined with anisotropic displacement parameters. Positions of hydrogen atoms were calculated using a riding model. Compound 3: Triclinic space group  $P\bar{1}$  (no. 2),  $a = 11.3770(4)$  Å,  $b = 12.1632(5)$  Å,  $c = 14.5978(6)$  Å,  $\alpha = 104.636(2)^\circ$ ,  $\beta = 96.217(2)^\circ$ ,  $\gamma = 113.276(2)^\circ$ ,  $V = 1745.50(12)$  Å<sup>3</sup>,  $Z = 2$ ,  $\rho_{\text{calcd}} = 1.461$  g/cm<sup>3</sup>,  $T = 233$  K,  $\mu = 0.521$  mm<sup>-1</sup>, orange prism, 6121 reflections  $> 2\sigma(I)$ ,  $R_1 = 0.0350$ , and  $\omega R_2 = 0.0804$ . Compound 6a: Triclinic space group  $P\bar{1}$ ,  $a = 10.2007(4)$  Å,  $b = 13.8886(4)$  Å,  $c = 14.9130(6)$  Å,  $\alpha = 107.497(2)^\circ$ ,  $\beta = 94.569(2)^\circ$ ,  $\gamma = 95.552(2)^\circ$ ,  $V = 1992.37(13)$  Å<sup>3</sup>,  $Z = 2$ ,  $\rho_{\text{calcd}} = 1.605$  g/cm<sup>3</sup>,  $T = 233$  K,  $\mu = 0.993$  mm<sup>-1</sup>, orange prism, 6844 reflections  $> 2\sigma(I)$ ,  $R_1 = 0.0282$ , and  $\omega R_2 = 0.0648$ . Compound 7: Monoclinic space group  $C2/c$  (no. 15),  $a = 27.0985(3)$  Å,  $b = 14.4321(4)$  Å,  $c = 20.3053(5)$  Å,  $\beta = 109.654(2)^\circ$ ,  $V = 7478.5(3)$  Å<sup>3</sup>,  $Z = 8$ ,  $\rho_{\text{calcd}} = 1.413$  g/cm<sup>3</sup>,  $T = 233$  K,  $\mu = 0.528$  mm<sup>-1</sup>, orange prism, 5820 reflections  $> 2\sigma(I)$ ,  $R_1 = 0.0348$ , and  $\omega R_2 = 0.0784$ . Compound 8: Orthorhombic space group  $P2_12_12_1$  (no. 19),  $a = 10.8932(2)$  Å,  $b = 16.4398(4)$  Å,  $c = 26.9136(7)$  Å,  $\alpha = \beta = \gamma = 90^\circ$ ,  $V = 4819.74(19)$  Å<sup>3</sup>,  $Z = 4$ ,  $\rho_{\text{calcd}} = 1.414$  g/cm<sup>3</sup>,  $T = 233$  K,  $\mu = 0.506$  mm<sup>-1</sup>, colorless prism, 6183 reflections  $> 2\sigma(I)$ ,  $R_1 = 0.0548$ , and  $\omega R_2 = 0.1203$ . Compound 9: Orthorhombic space group  $P2_12_12_1$ ,  $a = 10.8403(2)$  Å,  $b = 16.5038(3)$  Å,  $c = 27.1075(4)$  Å,  $\alpha = \beta = \gamma = 90^\circ$ ,  $V = 4849.70(14)$  Å<sup>3</sup>,  $Z = 4$ ,  $\rho_{\text{calcd}} = 1.408$  g/cm<sup>3</sup>,  $T = 233$  K,  $\mu = 0.503$  mm<sup>-1</sup>, colorless prism, 7510 reflections  $> 2\sigma(I)$ ,  $R_1 = 0.0461$ , and  $\omega R_2 = 0.1181$ .

**Supporting Information** (see footnote on the first page of this article): Comparison of the calculated most stable structure of **3** with its X-ray structure; the most stable structure of *endo*-**IIIb**-type Ru-alkylidene complexes; energy diagram and structures of the transition states for the H-shift from C1 to C2 for both *exo*-**3a** and *endo*-**3a**.

CCDC-631369 to -631371, -631373, and -631374 (for compounds **3**, **6a** and **7-9**) contain the supplementary crystallographic data for this paper. These data can be obtained free of charge from The Cambridge Crystallographic Data Centre via [www.ccdc.cam.ac.uk/data\\_request/cif](http://www.ccdc.cam.ac.uk/data_request/cif).

## Acknowledgments

Our work was supported by grants from the Deutsche Forschungsgemeinschaft (DFG, BU2174/2-1) and the Freistaat Sachsen.

- [1] R. H. Grubbs, *Handbook of Metathesis*, 1st ed., Wiley-VCH, Weinheim, **2003**, vols. 1–3.
- [2] T. M. Trnka, R. H. Grubbs, *Acc. Chem. Res.* **2001**, *34*, 18–29.
- [3] A. Hafner, A. Mühlebach, P. A. van der Schaaf, *Angew. Chem.* **1997**, *109*, 2213–2216; *Angew. Chem. Int. Ed. Engl.* **1997**, *36*, 2121–2123.
- [4] E. Lindner, S. Pautz, R. Fawzi, M. Steimann, *Organometallics* **1998**, *17*, 3006–3014.
- [5] A. Demonceau, A. W. Stumpf, E. Saive, A. F. Noels, *Macromolecules* **1997**, *30*, 3127–3136.
- [6] L. Jafarpour, J. Huang, E. D. Stevens, S. P. Nolan, *Organometallics* **1999**, *18*, 3760–3763.
- [7] L. Ackermann, C. Bruneau, P. H. Dixneuf, *Synlett* **2001**, *3*, 397–399.
- [8] D. Sémeril, C. Bruneau, P. H. Dixneuf, *Helv. Chim. Acta* **2001**, *84*, 3335–3341.
- [9] D. Sémeril, M. Cléran, C. Bruneau, P. H. Dixneuf, *Adv. Synth. Catal.* **2001**, *343*, 184–187.
- [10] D. Sémeril, C. Bruneau, P. H. Dixneuf, *Adv. Synth. Catal.* **2002**, *344*, 585–595.
- [11] R. Castarlenas, I. Alaoui-Abdallaoui, D. Sémeril, B. Mernari, S. Guesmi, P. H. Dixneuf, *New J. Chem.* **2003**, *27*, 6–8.
- [12] L. Delaude, A. Demonceau, A. F. Noels, *Chem. Commun.* **2001**, 986–987.
- [13] L. Delaude, M. Szypa, A. Demonceau, A. F. Noels, *Adv. Synth. Catal.* **2002**, *344*, 749–756.
- [14] Y. Zhang, D. Wang, P. Lönnecke, T. Scherzer, M. R. Buchmeiser, *Macromol. Symp.* **2006**, *236*, 30–37.
- [15] T. Ung, A. Hejl, R. H. Grubbs, Y. Schrodi, *Organometallics* **2004**, *23*, 5399–5401.
- [16] A. Hejl, M. W. Day, R. H. Grubbs, *Organometallics* **2006**, *25*, 6149–6154.
- [17] P. A. van der Schaaf, R. Kolly, H. J. Kirner, F. Rime, A. Mühlebach, A. Hafner, *J. Organomet. Chem.* **2000**, *606*, 65–74.
- [18] A. Hafner, P. van der Schaaf, A. Mühlebach, P. Bernhard, U. Schaedeli, T. Karlen, A. Ludi, *Prog. Org. Coat.* **1997**, *32*, 89–96.
- [19] G. Bhukta, R. Manivannan, G. Sundarajan, *J. Organomet. Chem.* **2000**, *601*, 16–21.
- [20] B. Gita, G. Sundararajan, *J. Mol. Catal. A* **1997**, *115*, 79–84.
- [21] J. O. Krause, M. T. Zarka, U. Anders, R. Weberskirch, O. Nuyken, M. R. Buchmeiser, *Angew. Chem.* **2003**, *115*, 6147–6151; *Angew. Chem. Int. Ed.* **2003**, *42*, 5965–5969.
- [22] J. O. Krause, O. Nuyken, M. R. Buchmeiser, *Chem. Eur. J.* **2004**, *10*, 2029–2035.
- [23] J. O. Krause, D. Wang, U. Anders, R. Weberskirch, M. T. Zarka, O. Nuyken, C. Jäger, D. Haarer, M. R. Buchmeiser, *Macromol. Symp.* **2004**, *217*, 179–190.
- [24] T. S. Halbach, S. Mix, D. Fischer, S. Maechling, J. O. Krause, C. Sievers, S. Blechert, O. Nuyken, M. R. Buchmeiser, *J. Org. Chem.* **2005**, *70*, 4687–4694.
- [25] T. S. Halbach, J. O. Krause, O. Nuyken, M. R. Buchmeiser, *Macromol. Rapid Commun.* **2005**, *26*, 784–790.
- [26] T. S. Halbach, J. O. Krause, O. Nuyken, M. R. Buchmeiser, *Polym. Prepr. (Am. Chem. Soc., Div. Polym. Chem.)* **2005**, *46*, 615–616.
- [27] L. Yang, M. Mayr, K. Wurst, M. R. Buchmeiser, *Chem. Eur. J.* **2004**, *10*, 5761–5770.
- [28] M. R. Buchmeiser, F. Sinner, M. Mupa, K. Wurst, *Macromolecules* **2000**, *33*, 32–39.
- [29] K. Matyjaszewski, *Macromolecules* **1993**, *26*, 1787–1788.
- [30] C. W. Bielawski, R. H. Grubbs, *Angew. Chem.* **2000**, *112*, 3025–3028; *Angew. Chem. Int. Ed.* **2000**, *39*, 2903–2906.
- [31] J. O. Krause, K. Wurst, O. Nuyken, M. R. Buchmeiser, *Chem. Eur. J.* **2004**, *10*, 777–784.
- [32] G. K. Cantrell, S. J. Geib, T. Y. Meyer, *Organometallics* **2000**, *19*, 3562–3568.
- [33] J. Zhang, T. B. Gunnoe, *Organometallics* **2003**, *22*, 2291–2297.
- [34] J. D. Rule, J. S. Moore, *Macromolecules* **2002**, *35*, 7878–7882.
- [35] D. Wang, L. Yang, U. Decker, M. Findeisen, M. R. Buchmeiser, *Macromol. Rapid Commun.* **2005**, *26*, 1757–1762.
- [36] K. J. Ivin, J. Kress, J. A. Osborn, *J. Mol. Catal.* **1988**, *46*, 351–358.
- [37] E. Khosravi, A. A. Al-Hajaji, *Polymer* **1998**, *39*, 5619–5625.
- [38] E. Khosravi, A. A. Al-Hajaji, *Eur. Polym. J.* **1998**, *34*, 153–157.
- [39] R. A. Zelonka, M. C. Baird, *Can. J. Chem.* **1972**, *50*, 3063–3072.
- [40] A. D. Becke, *J. Chem. Phys.* **1993**, *98*, 5648–5652.
- [41] A. D. Becke, *J. Chem. Phys.* **1996**, *104*, 1040–1046.
- [42] C. T. Lee, W. T. Yang, R. G. Parr, *Phys. Rev. B: Condens. Matter* **1988**, *37*, 785–789.
- [43] *Jaguar*, Schrodinger LLC, New York, **2005**.
- [44] W. R. Wadt, P. J. Hay, *J. Chem. Phys.* **1985**, *82*, 284–298.
- [45] S. Fomine, S. M. Vargas, M. A. Tlenkopatchev, *Organometallics* **2003**, *22*, 93–99.
- [46] S. Fomine, J. V. Ortega, M. A. Tlenkopatchev, *J. Mol. Catal. A* **2005**, *236*, 156–161.
- [47] S. Fomine, J. V. Ortega, M. A. Tlenkopatchev, *Organometallics* **2005**, *24*, 5696–5701.
- [48] B. F. Straub, *Angew. Chem.* **2005**, *117*, 6129–6132; *Angew. Chem. Int. Ed.* **2005**, *44*, 5974–5978.
- [49] Z. Otwinowski, W. Minor, *Methods in Enzymology*, Academic Press, New York, **1997**, vol. 276.
- [50] G. M. Sheldrick, *Program package SHELXTL V.5.1*, Bruker Analytical X-ray Instruments Inc, Madison, USA, **1997**.

Received: January 12, 2007  
Published Online: July 6, 2007